Satellite Estimation of the Surface Energy Balance, Moisture Availability and Thermal Inertia

TOBY N. CARLSON, JOSEPH K. DODD,[1] STANLEY G. BENJAMIN AND JAMES N. COOPER

Department of Meteorology, The Pennsylvania State University, University Park 16802

(Manuscript received 17 March 1980, in final form 23 August 1980)

ABSTRACT

A method for inferring the distribution of surface heat and evaporative fluxes and the ground moisture availability and thermal inertia (ground conductive capacity) is used to analyze two urbanized areas, Los Angeles and St. Louis. The technique employs infrared satellite temperature measurements in conjunction with a one-dimensional boundary-layer model. Results show that there is a marked reduction of evaporation and moisture availability and a corresponding elevation of sensible heat flux over urbanized areas and over cropped areas with low vegetative cover. Conversely, low heat flux and high evaporation characterize vegetated and, especially, forested areas. Warm urban centers appear directly related to a reduction in vegetation, which normally allows for a greater fraction of available radiant energy to be converted into latent heat flux. The distribution of thermal inertia was surprisingly ill-defined and its variation between urban and rural areas was quite small. Thus, the increased heat storage within the urban fabric, which has been proposed as the underlying cause of the nocturnal heat island, may be caused mainly by enhanced daytime surface heating which occurs because of surface dryness, rather than by large spatial variations in the conductivity of the surface.

1. Introduction

One of the most notable meteorological anomalies produced by human activity is the urban heat island. Many studies (e.g., Duckworth and Sandberg, 1954; Landsberg, 1956; Oke, 1968; Chandler, 1976) show urban-rural temperature differences of several degrees Celsius with the greatest elevations in ground and air temperatures occurring during the evening hours. Recent investigations into the phenomenon have begun to focus attention on the significance of differential heating patterns in altering the amount and type of precipitation surrounding urban areas. Earlier studies of urban precipitation anomalies led to various hypotheses concerning the possible anthropogenic effects on the weather (Changnon, 1969). The results of METROMEX (Braham and Dungey, 1978; Braham and Wilson, 1978; Huff and Vogel, 1978; Changnon, 1969, 1978) indicate that there are significant precipitation anomalies in the vicinity of St. Louis, which are connected with convective situations during the summer months. Moreover, these studies show clearly that strong convergence of the low-level wind occurs over the hottest portions of the city (Kropfli and Kohn, 1978; Wong and Dirks, 1978; Shreffler, 1979). Both observational and theoretical investigations indicate that surface heat flux must be considered in modeling small-scale circulation patterns in regions of differential surface heating.

Models capable of predicting the surface temperature response and the amount of surface heating are in wide use, both as components within larger hydrodynamic models or as separate one-dimensional entities whose purpose is to study the nature of surface heating by itself. Various types of one-dimensional surface temperature models have been developed [see, e.g., Myrup (1969), Outcalt (1972), Rosema (1979), Carlson and Boland (1978, hereafter referred to as CB), Deardorff (1978), Blackadar (1979) and Soer (1977; 1980)].

In applying any model, however, it is possible to simulate any desired surface temperature response by appropriately setting the model parameters. Over heterogeneous terrain such as an urban-rural complex, the concepts of conductivity or moisture availability are difficult to measure directly. Yet, it is certainly evident that the ability of a particular surface to transpire or to conduct heat internally must be represented in a physically realistic manner in order to predict the surface temperature. Certainly, radiometric surface temperature observations over urban and rural areas indicate that the surface heating is strongly influenced by the composition of the surface.

In many numerical models of the surface, an important constraint imposed on the solution of the

[1] Present affiliation: Aerospace Corporation, Los Angeles, CA 90009.

0021-8952/81/010067-21$09.25

equations is a surface energy balance. In such formulations, surface heat flux and surface temperature are intimately related; thus, the partitioning of energy into sensible and latent heat is directly reflected in the amplitude and nature of the surface temperature wave. The greatest amplitude of the temperature wave occurs immediately at the ground-air interface and decreases very rapidly with height both upward and downward from the interface. Well away from the surface, in the atmosphere, the diurnal temperature fluctuations are likely to be much weaker than at the surface and are greatly modulated by advection and other meteorological influences. Thus the surface temperature response, as a highly sensitive measure of the surface character, reflects the nature of that surface in a way which might allow one to distinguish a road surface from grass, dry soil from wet soil or trees from buildings.

Rather than measure the surface parameters which govern the temperature response, we would prefer to conceive of these parameters as *effective* values which we now define as being those values that yield exactly and uniquely the observed temperature response at the surface within a model; thus, they constitute solutions to the model for the measured surface temperatures. This paper considers a method proposed by CB for determining values for the governing parameters of the surface temperature response. Our approach is to use the measured radiative surface temperatures, in this case from a satellite, in conjunction with a rather general one-dimensional boundary-layer model, to infer the surface energy fluxes and the ground parameters. CB showed that given two surface temperature observations, preferably near the times of maximum and minimum temperatures, it is possible to infer the values of two model parameters, the moisture availability and thermal inertia, which are the essential governing parameters in the surface energy budget.

The concept of inferring the thermal properties of a surface using infrared radiometric measurements in conjunction with a surface model arises from methods used by geologists to study the thermal properties of rock and mineral formations (Kahle, 1977). In a study of the St. Louis heat island, Dabberdt and Davis (1978) used a one-dimensional surface heat flux model in conjunction with aircraft radiometric measurements to infer the ground thermal inertia and Bowen ratio along aircraft tracks across the city. Recently, various European investigators (Soer, 1977, 1980) have developed a highly similar modeling approach to that of CB. Their method utilizes satellite-derived day-night satellite temperature differences to infer values of the surface fluxes, the surface relative humidity and the thermal inertia in the manner similar to that described in this paper.

As shown by CB, errors made in determining other model parameters, such as the measured wind speed, the ground albedo or emissivity, surface roughness and atmospheric turbidity, are partly compensating and will lead, in the calculations of surface temperature and heat flux, to errors of less than $\pm 2°C$ and 30%, respectively. Such errors are acceptable for satellite applications because it is not possible to measure remotely the temperature to within a relative accuracy of much less than $\pm 2°C$, because of spatial variations in ground emissivity. However, the satellite provides the advantageous feature in being able to average a signal from a large number of surface emittors and reflectors, thus yielding a single area-averaged value of temperature.

A possible source of uncertainty in applying a one-dimensional model is the neglect of advection. Although we have confined our attention to cases of light winds, advection cannot be discounted as long as there are horizontal surface heating variations. It is clear, however, from an examination of the surface temperature maps and also of the derived energy fluxes (as, for example, are presented in this paper), that strong horizontal gradients in the measured ground temperature (and thus in the surface heat flux) are preserved despite the smoothing effects of advection. For example, not only are sharp temperature and heat flux gradients found along the Los Angeles coastline in the presence of a prevailing sea breeze, but we have discovered no systematic gradient in the surface temperatures between coastal urban areas and the urbanized areas in the interior of Los Angeles. Thus, one can say that a relatively hot surface, whether situated near the coast or not, will be detected as such by a radiometer viewing that surface from an aircraft or from a satellite. Accordingly, such relative warmth will correspond to a relatively elevated surface heat flux in the model, with no serious degradation of the results due to advection.

In this paper we will apply a recent version of the CB model in conjunction with satellite measurements to infer the moisture availability, thermal inertia, and the surface energy balance over two urban areas. In the next sections, we will outline the structure of the model, the system for processing and manipulating the satellite data, and the method by which the satellite measurements are substituted into regression equations determined from results of the model to yield the surface parameters and the surface fluxes. Finally, some analyses of these fields will be presented for two case studies.

2. The surface model

a. Daytime model

The basic structure of the surface temperature model is described by CB. It consists of four layers: a mixing layer, a 50 m surface turbulent layer, a

thin transition layer between the air and the surface interface, across which diffusive fluxes at the interface are passed to the turbulent layer, and a 1 m ground layer (Fig. 1). The transition layer is viewed as a layer that contains many surface obstacles. Across the layer there is a variation between purely turbulent and purely molecular flow where radiation, conduction and turbulent heat transfer coexist in some fashion.

The underlying constant in the model is the energy balance at the surface air interface

$$R_n = G_0 + H_0 + E_0 = (1 - A_0)S - \epsilon_g \sigma T_0^4 + \epsilon_a \sigma T_a^4, \quad (1)$$

where G_0, H_0 and E_0 represent, respectively, the sensible heat flux into the ground, the sensible heat flux into the atmosphere; and the latent heat flux into the atmosphere. Net radiation R_n is calculated from a radiation balance at the surface [the right side of (1)], where A_0 is the surface albedo, T_0 the temperature at the ground air interface, σ the Stephan-Boltzmann constant, and T_a the temperature at the top of the surface layer (z = 50 m). Net solar flux (direct plus diffuse) S is calculated from a one-layer solar-radiation model (Carlson and Boland, 1978). Emissivity at the ground is set equal to 1.0, but that for the atmosphere ϵ_a is calculated from a formula suggested by Monteith (1961) in which thermal back radiation is represented as a function of the total precipitable water ω in the atmospheric column, $\epsilon_a = 0.725 + 0.17 \log_{10} \omega$, where ω is in centimeters. Surface flux of sensible heat is parameterized in the surface layer, over which H_0 is presumed to be constant, as

$$H_0 = -(C_h + \rho c_p K_h) \frac{\partial \theta}{\partial z}, \quad (2)$$

where K_h is the eddy diffusivity, C_h a heat transfer coefficient for nonturbulent heat flux in the surface transition layer, c_p the specific heat at constant pressure for dry air, and ρ the air density. The potential temperature θ is normalized to surface pressure at the ground-air interface; thus $\theta_0 = T_0$. Integrating (2) with respect to z from the ground to the top of the surface layer at z_a, where $\theta = \theta_a$ yields

$$\theta_0 \equiv T_0 = \theta_a + H_0 I_h / \rho c_p, \quad (3)$$

where I_h is essentially a resistance coefficient determined from an integration of the generalized height-dependent diffusivity $K(z) = K_h + C_h/\rho c_p$.

A similar equation to (3) for water vapor flux is

$$E_0 = \frac{\rho L_e}{I_q} M[q_{0s}(T_0) - q_a], \quad (4)$$

where I_q for water vapor is identical to that for heat except that the diffusivities refer to those of water vapor, K_q and C_q. In all calculations K_q was assumed

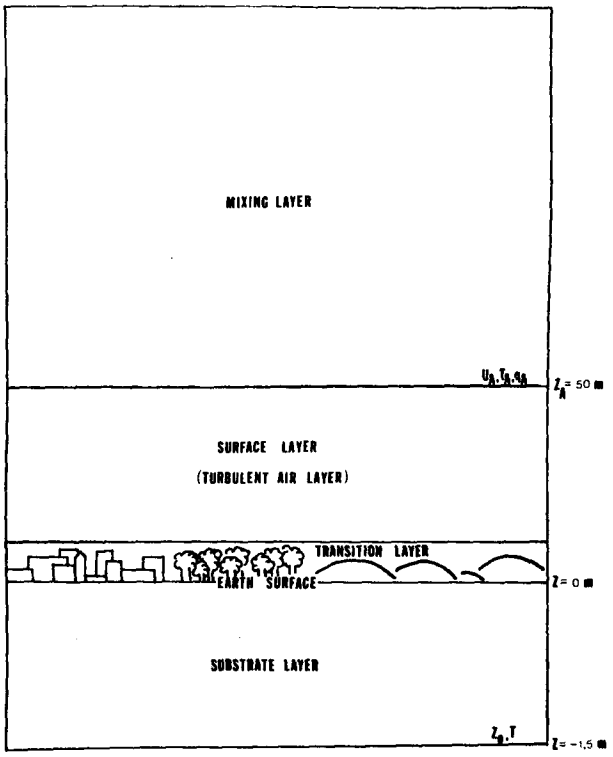

FIG. 1. Basic structure of model.

to be equal to K_h, but C_h and C_q were assigned, for lack of a better choice, values for the molecular diffusivities of heat and water vapor. Justification for use of molecular diffusivity in the context is discussed by Garratt (1978). Here, $q_{0s}(T_0)$ and q_a are, respectively, the saturation specific humidity at the surface and the specific humidity at z_a, the top of the surface layer; L_e is the latent heat of vaporization, and M is called the *moisture availability*. The concept of moisture availability was suggested by Tanner and Pelton (1960) and later elaborated on by Nappo (1975). This parameter basically expresses the efficiency of surface evaporation and is the fraction of maximum possible evaporation for a saturated surface at temperature T_0. The moisture availability can be conceived as a measure of water saturation at ground surface. For vegetation, M is related to the internal resistance (bulk stomatal diffusion resistance) discussed by Monteith (1975).

The ground surface flux G_0 is given by the standard conduction equation

$$G_0 = \lambda(T_0 - T_{-1})/\Delta Z, \quad (5)$$

where λ is the thermal conductivity of the substrate and T_{-1} the temperature of the first substrate level, a distance ΔZ below the ground surface. The transfer of heat through the soil is governed by the diffusion equation. Assuming a homogeneous substrate layer,

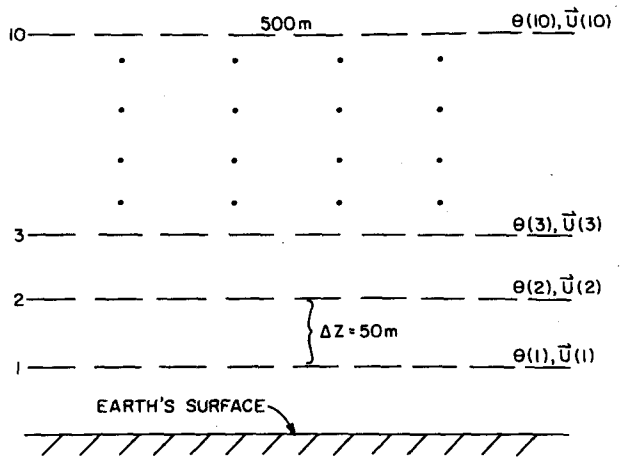

FIG. 2. Basic structure of nocturnal component of model.

$$\frac{\partial T}{\partial t} = \kappa \frac{\partial^2 T}{\partial Z^2}, \tag{6}$$

where κ is the thermal diffusivity of the substrate, identical to λ/C_g, C_g being the ground heat capacity.

b. Nighttime model

During the daytime, specifically under unstable conditions ($H_0 > 0$) when there is solar heating of the surface, the surface-layer stability profile is largely determined by the intensity of surface heating and by constraints of Monin-Obukov scaling. When the solar flux diminishes to the point where H_0 becomes negative, the turbulence represented by the friction velocity, u_* begins to diminish rapidly. During stable conditions, the temperature profile is strongly affected by the longwave radiational cooling and by the vertical wind shear near the surface. Heat flux no longer is determined directly by net radiation but becomes passively dependent on the lapse rate. As the surface layer becomes more stable with time, the downward heat flux and u_* both tend to vanish or to become intermittent.

To account for the nighttime regime, a modified form of the Blackadar (1979) critical Richardson number approach, differing from the original CB model, is used. In the Blackadar scheme, the maintenance of turbulence under nocturnal conditions is governed by a bulk Richardson number Ri_B, which, for the surface layer, is given by

$$\mathrm{Ri}_B = \frac{g z_a}{\bar{\theta} W_a^2} [(\theta_a - \theta_s) + T_* \ln(z_a/z_0)], \tag{7}$$

where W_a is the total wind speed at z_a, $\bar{\theta}$ is the average temperature in the surface layer, g the gravitational constant and θ_s a "shelter" height temperature (nominally at 1 m) which is predicted using the equation

$$\frac{\partial \theta_s}{\partial t} = a(\theta_0 - \theta_s) - b \frac{H_0}{\rho c_p z_a}. \tag{8}$$

Eq. (8) is an empirical relationship incorporating two terms on the right side. The first term is meant to simulate radiative conduction and radiational cooling in the lowest meter. The second term simulates a temperature change due to turbulent flux itself. Values for the constants, suggested by Blackadar, are $a = 8.3 \times 10^{-4}\ \mathrm{s}^{-1}$ and $b = 0.2$. At equilibrium, the two terms on the right side of (8) cancel, heat flux convergence balancing radiative divergence. Monin-Obukov scaling is used to define T_* and u_* where

$$T_* = (\theta_a - \theta_s)/[\ln(z_a/z_s - \psi_h)], \tag{9a}$$

$$u_* = kW_a/[\ln(z_a/z_0 - \psi_m)], \tag{9b}$$

$$H_0 = -k\rho c_p u_* T_*, \tag{9c}$$

where θ_a and z_a have their usual meaning for the surface layer. Here, ψ_h and ψ_m are the nondimensional profiles for temperature and wind, the functional forms of which are dependent on stability, and k is the von Kármán constant.

The vertical profiles for temperature and wind from 50 to 500 m are provided through the integration of the u and v momentum equations and the thermodynamic equation, expressed as

$$\frac{\partial u_i}{\partial t} = f(v_i - v_{gi}) + \frac{K_{mi+1}}{\Delta z^2}(u_{i+1} - u_i) - \frac{K_{mi}}{\Delta z^2}(u_i - u_{i-1}), \tag{10}$$

$$\frac{\partial \theta_i}{\partial t} = \frac{K_{hi+1}}{\Delta z^2}(\theta_{i+1} - \theta_i) - \frac{K_{hi}}{\Delta z^2}(\theta_i - \theta_{i-1}) + \frac{\Delta \theta_R}{\Delta t}, \tag{11}$$

where f is the Coriolis parameter, Δz the layer depth in the atmosphere (50 m), $\Delta\theta_R$ a small correction for radiative cooling, and subscript i is the level index, which varies from 1 (at $z = z_a = 50$ m) to 10 (at $z = 500$ m) as in Fig. 2. The v momentum equation (not shown) is exactly analogous to (11). The eddy exchange coefficients K_h and K_m are assumed to be equal in the stable nocturnal boundary layer and are expressed by the function

$$K_i = l^2 S_i \frac{(\mathrm{Ri}_c - \mathrm{Ri})}{\mathrm{Ri}_c} \tag{12}$$

which was found by Blackadar (1979) to fit the data of Mellor and Yamada (1974) for second-order closure theory. In (13),

$$S_i = [(u_i - u_{i-1})^2 + (v_i - v_{i-1})^2]^{1/2}/\Delta z \tag{13}$$

and l was arbitrarily chosen as 28 m in the surface layer. In the layers above the surface, the local Richardson number is calculated as

$$\mathrm{Ri} = \frac{g}{\bar{\theta}\Delta z}\frac{(\theta_i - \theta_{i-1})}{S_i^2}, \quad (14)$$

while the critical Richardson number (Ri_c) is calculated as a function of the geostrophic wind speed using an empirical result suggested by Blackadar[2]

$$\mathrm{Ri}_c = 0.5542 \exp\{-[0.2129(u_{gi}^2 + v_{gi}^2)^{1/2}] + 0.2\}, \quad (15)$$

where u_{gi} and v_{gi} are the geostrophic wind speed components in meters per second. When the local Richardson number exceeds the critical value, turbulent exchange will cease at that height and K_i is arbitrarily set equal to zero.

The lowest 50 m layer must be treated differently as there will be no turbulent exchange through the underlying surface. Accordingly, the last term in each equations (10) and (11) must be replaced by $-u_*^2 u_1/W_A\Delta z$ and $H_0/c_p\rho\Delta z$, respectively, which are the surface boundary flux conditions.

c. *Initial conditions*

The temperature at the bottom of the 1 m ground slab was set equal to constant, which was a representative climatological value. Above the surface layer, the mixing layer of depth h, potential temperature θ_a and mixing ratio q_a were allowed to vary during the daytime according to a model of Tennekes (1973) in which the mixing-layer parameters responded to an addition of sensible heat flux from the ground and an entrainment of higher potential temperature from above the mixing layer. Thus, the temperature and moisture at the top of the surface layer were determined by the amount of surface heating and the stability and moisture distribution above the surface layer. The wind speed u_a, however, was not calculated from Eq. (10). Instead, a 500 m layer above the surface layer was presumed to be well mixed with u_a constant up until the time of late afternoon stability reversal, a reasonable assumption for a clear sunny day. The nighttime model became effective when H_0 became zero in the late afternoon; subsequently, the wind and temperature profiles were calculated from (10) and (11) over the 500 m deep layer at equal intervals of 50 m from $i = 1$ at z_a to $i = 10$ at $z = 500$ m (Fig. 2). Although the model was usually started near dawn, the initial wind profile was determined from a late afternoon or early evening wind sounding when the stability would have been close to neutral. The procedure for initializing the wind profile and for obtaining u_a was as follows: The vertical shear of the geostrophic wind was determined from an analysis of local surface fields of temperature and pressure; usually only one or two additional wind observations above the surface layer were available in the lowest 500 m. In order to fit a wind profile to the observations, free convection scaling was assumed to govern the wind profile prior to the vanishing of the upward heat flux. The assumption of free convection scaling assumes that turbulence in the lower part of the mixed layer is buoyantly driven (Tennekes, 1970), and provides a relationship for the wind shear

$$\frac{\partial V}{\partial z} = b' z^{-4/3}. \quad (16)$$

This leads to a velocity defect expression

$$V - V_{\mathrm{obs}} = b'(z^{-1/3} - z_{\mathrm{obs}}^{-1/3}), \quad (17)$$

where b' is determined empirically and z is measured downward from z_{obs}, the level where the wind speed V is equal to V_{obs}. Eq. (17) is applied to 0000 GMT wind data for the layer between the top of the surface layer at 50 m and z_{obs} which was taken at 200 m. The wind at 200 m was either a measured wind close to that level or was assumed to be equal to the surface geostrophic wind. Above 200 m the wind was assumed to be initially constant with height to 500 m. The specified initial wind profile may possess a significant ageostrophic component, but the model has been found to adjust smoothly to the transition during the first hour or two of integration beyond the time of reversal in the sign of the heat flux, ultimately achieving a quasi-equilibrium with small accelerations.

d. *Solution of the model*

During the daytime the surface heat flux is obtained by a solution to the surface energy budget (1). The temperature at the surface is determined from the heat flux in accordance with the stability prescribed by (3). Given prescribed values for all of the terrain parameters and an initial temperature and wind profile within the atmosphere above the surface and within the ground, the essential unknowns H_0, T_0, T_{-1}, E_0 and G_0 can be found using Eqs. (1), (3), (4), (5) and (6). Because many of the terms are interdependent, it was necessary to cycle through the system of equations until convergence was achieved. Values of the eddy diffusivities were cal-

[2] Private communication. This relationship is based on a comparison of field measurements of wind made at O'Neill, Nebraska, and Wangara with those obtained from the Blackadar (1979) slab model. Under light wind conditions there is a greater likelihood of finding thin layers where wind shear and temperature vary rapidly with height. If Δz is too large to resolve this, the calculated Ri may be far larger than the smallest value in the layer and thus turbulence can still occur even though the calculated $\mathrm{Ri} > 0.2$. The equation systematically accounted for the bias found when the measurements were compared with the model results.

culated from Monin-Obukov theory using the heat flux and lapse rate determined from the previous time step with neutrality assumed at $t = 0$. Choosing a time step of 4 min during the day and 2 min at night not only insured stability of solutions but also resulted in slowly varying values of the fluxes and temperature between time steps, necessitating only one iteration per time step.

Heat flux was calculated first. As in CB, Eqs. (1), (3), (5) and (6) were combined to form an expression for H_0. The wind speed and friction velocity u_* were used to solve for I_h and I_q. The momentum profile was solved between the limits z_0, which is the effective roughness height for momentum, and z_a using the nondimensional momentum profiles for ϕ_m. The effective roughness heights for momentum or for heat (z_l) were considered to be some unspecified distance above a zero displacement plane height, rather than at true ground surface. After determining H_0, T_0 was determined from (3) followed by the fluxes E_0 and G_0. Finally, the substrate temperature profile was determined from (6).

The solution to the model at night differed from that during the day in that the heat flux was calculated directly from (9c) and therefore was determined from the near-surface stability, which was predicted by time-dependent equations (8), (10), (11) using the relationships (7), (12), (13) and (14), and subject to the constraints of the critical Richardson number formulation. Given the heat flux, surface temperature was then determined as an equilibrium solution to the energy balance (1). Evaporative flux was calculated from (4) until it became negative and then was set to zero. Ground flux and the substrate time rate of change of temperature were still calculated from (5) and (6).

The value of the bulk Richardson number defines three stability classifications for which events in the surface layer will be quite dissimilar:

(I) $\mathrm{Ri}_B < 0$, unstable

(II) $0 \leq \mathrm{Ri}_B \leq 0.2$, stable

(III) $\mathrm{Ri}_B > 0.2$, non-turbulent.

In cases I and II, the surface heat flux is given by Eq. (9) and will be positive when the surface layer is unstable (a situation which will rarely occur at night), and negative (downward directed) when stable. For case III the surface layer will be decoupled from events at and above 50 m because of the strongly stable lapse rate near the ground ($\theta_a > \theta_0$); both u_* and H_0 will then become zero. The progression of events from neutral stability to non-turbulent radiation equilibrium (case III) has been described by Blackadar (1979).

The primary purpose in predicting these turbulent events is to achieve a more realistic surface temperature. The governing parameter for these events is the geostrophic wind (assumed constant with time). On nights when the surface geostrophic wind is large, turbulent events are more likely. Unlike the daytime case, q_a was not allowed to vary under stable conditions and is thus held constant throughout the night.

Because the integral I_h in (3) and I_q in (4) undefined when turbulence ceases, the energy balance at the surface was used directly to solve for the surface temperature when H_0 became negative although E_0 continued to be determined from (4) until it became negative. I_h and I_q were actually constrained from becoming zero by setting 1.0 cm s^{-1} as a lower limit for u_*.

Solving for T_0 in (1) yields the quartic equation

$$A'T_0^4 + B'T_0 + C' = 0, \tag{18a}$$

where

$$A' = \epsilon_g\sigma, \tag{18b}$$

$$B' = \lambda/\Delta Z, \tag{18c}$$

$$C' = \lambda T_{-1}/\Delta Z + H_0 + E_0 - \epsilon_a\sigma T_a^4 + S. \tag{18d}$$

At each time step, Newton's iterative technique for finding real zeros of a polynomial is used to solve for T_0. At night in the non-turbulent surface layer H_0, E_0 and S are zero so that Eq. (18) expresses a balance between the longwave terrestrial radiation and the ground heat flux. As such, the value of λ, the thermal conductivity, is an important factor in the nighttime behavior of T_0.

The substrate diffusivity and conductivity or the conductivity, density ρ_g and specific heat c_s ($\rho_g c_s = c_g$) of the substrate are combined to form a parameter called the *thermal inertia* P, where

$$P = \lambda\kappa^{-1/2} = (\lambda c_g)^{1/2} \tag{19}$$

is a measure of the rate of heat transfer at the ground-air interface. P is also called the thermal admittance or conductive capacity of the ground medium. As defined here, the thermal inertia has been shown by Lettau (Sellers, 1965) to be inversely proportional to the amplitude of the first harmonic of the ground heat flux into the soil.

Tests with the model show that the results are fairly insensitive to the exact choices of either λ or κ for a given value of P. Thus, thermal inertia appears to be a more fundamental measure of the ground conductivity of diffusivity, replacing both of these difficult-to-measure quantities by a single parameter. Since both λ and κ (rather than P) are used explicitly in the model, we adopted a convention for equating P with λ and κ. This convention proved to be necessary because, although independent variations in λ and κ generally yielded identical results for constant values of P, when λ and κ were assigned extreme values the results no longer were unchanged for the same value of P. Accordingly, the formula

$$\lambda[\text{cal cm}^{-1}\ \text{K}^{-1}\ \text{s}^{-1}] = -0.00013 + 0.0502P + 1.21P^2[\text{cal cm}^{-2}\ \text{K}^{-1}\ \text{s}^{-1/2}] \quad (20)$$

was used as a constraint on the value of λ in the model.[3] Eq. (20) was determined by fitting a second-order regression equation through 20 pairs of λ and P values listed in Sellers (1965) and in the *Manual of Remote Sensing, II* (1975). The regression was found to explain 91% of the variance of λ about P in the dependent data sample, providing an empirical result which corresponds to a wide variety of surface materials. In fact, the actual surface canopy may consist of materials which may not represent a truly diffusing or conducting medium, such as a mixture of structures and vegetation—trees, roads, houses, crops, etc.

It is customary in surface layer modeling to specify the terrain parameters in order to calculate the surface temperature and the surface energy fluxes. Although we have shown that this can be done, it is the purpose of this paper to demonstrate how the model can be used to infer values for M and P and the surface fluxes, given measurements of the surface temperature. CB show that by supplying two surface temperatures in the same temperature cycle, two terrain parameters could be treated as unknowns whose values could be inferred with some uniqueness from iterative solutions of the mode. The method for inverting the model to obtain the terrain parameters given the surface temperatures is described in Section 4.

3. Reduction and analysis of satellite temperature measurements

During the past decade, several meteorological satellites with the capacity to provide high-resolution thermal mapping of the earth's surface have been placed in orbit. Polar orbiting vehicles, however, are incapable of scanning more than twice in a diurnal temperature cycle, and, until recently, the passes were made at hours shortly after sunrise and sunset. On 26 April 1978, the Heat Capacity and Mapping Mission (HCMM) polar-orbiting satellite was launched by NASA to provide high-resolution (~600 m) measurements of the radiometric ground temperature for application to ground-sensing problems. The noise equivalent temperature error (NEΔT) for this satellite is considered to be 0.3 K.[4] This satellite was able to scan a given location twice a day (at intervals of 16 days) at times very close to those of local maximum and local minimum temperature, approximately 1330 and 0230 LST, respectively. [More recently, the polar orbiting TIROS-N was launched into an orbit which allows for data acquisiton at about 1500 and 0300 LST and has a resolution of ~1100 m at zero scan angle (satellite directly overhead) and a NEΔT of 0.1 K.]

Satellite detection of heat islands has become possible only since the recent advent of high-resolution infrared window measurements. Although techniques for performing densitometric or radiometric analyses of small-scale temperature variations from aircraft date have been applied widely to the study of urban and other types of terrain (*Manual of Remote Sensing, II*; 1975); Rao (1972) was the first person to publish an account of the heat island using satellite data. Recently, it has been shown (Carlson *et al.*, 1977; Matson *et al.*, 1978) that the heat island is a relatively widespread phenomena.

The procedure which we followed for taking the raw HCMM satellite radiance data and coverting the information to temperature maps on a fixed geographical grid was as follows:

1) Digital count information for an area covered by a 512 × 512 matrix of data points (pixels) was extracted from raw data tape.

2) A 130 × 130 working area (~80 km on a side) was selected from within the larger matrix. A histogram of the count value was made and the data field printed out as an alphanumeric character map; an example of the type of output is shown by Chen *et al.* (1979).

3) Inspection of the character map compared with a topographic map enabled us to identify specific geographic features within the working area. These features were assigned values of x, y coordinates within an arbitrary geographically fixed reference frame which we call the "topo" grid.

4) The digital count (DN) values were converted to temperature using the appropriate calibrations. A spatially constant water vapor correction (Cogan and Willand, 1976) was applied. Moisture data was obtained from radiosonde information taken within or near the city.

5) Temperature analyses for both the daytime and night time orbits were rectified to the topo coordinates. A pair of temperatures, one day and one night value, were located at each x, y coordinate of a subset area.[5] All analyses were subjected to a simple one-pass smoothing.

4. Combining of model output with satellite data

As mentioned in Section 1, satellite temperature measurements were used in conjunction with

[3] In some papers thermal inertia is presented in thermal inertia units (TIU), which are W m^{-2} K^{-1} s$^{1/2}$. Approximately 400 TIU are equivalent to 0.01 cal cm^{-2} K^{-1} s$^{-1/2}$, the units presented in this paper.

[4] The authors recently became aware of a temperature offset error of ~5°C which must be added to all the HCMM temperature measurements to make them correct. Further analyses with the corrected temperatures indicate that the values of M and E_0 should be somewhat smaller and the value of P and H_0 somewhat larger than reported in this paper, although because of the energy balance constraint, the patterns appear little affected by making this correction.

[5] The location error of the data within the "topo" grid is about ±1 pixel (~600 m for HCMM).

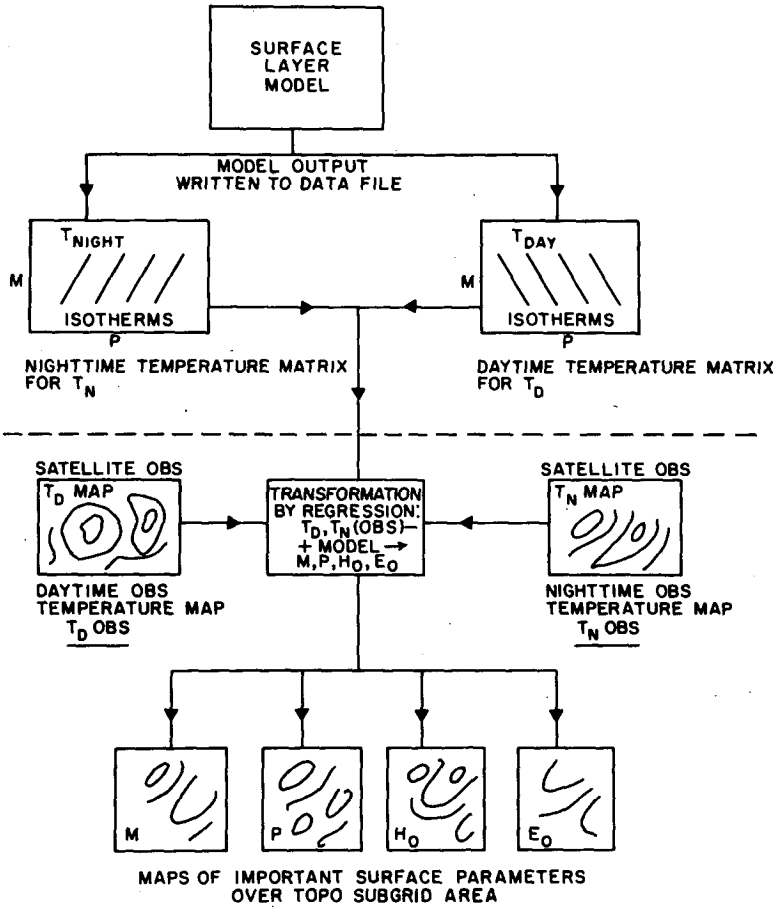

FIG. 3. Flow diagram for inferring surface parameters.

the model results to determine maps of moisture availability M, thermal inertia P, and the surface heat fluxes H_0 and E_0 (Fig. 3). Because of the complexity of interactions between the boundary layer and the surface, it was necessary to quantify the relationships between the aforementioned quantities and the surface temperatures with a series of regression equations determined from model output. Typically, the model was initialized at a time near sunrise and allowed to proceed for about a 22 h interval. Initial values of wind speed, temperature and moisture were obtained from local soundings and representative values for albedo, roughness and turbidity were included in the model. It was assumed that the various terrain parameters did not change throughout the day and thus represented daily averages.

Solutions of the model were generated by cycling through a 22 h period with equal incremented values of M and P until 16 daily temperature cycles were completed over the maximum likely ranges for M (0.05–1.0) and P (0.005–0.1).[6] At two specified times during each of these cycles, corresponding to times of day and night satellite passes, the model results were extracted, stored and, subsequently, used to determine a set of regression equations with surface temperatures as predictors, and the surface fluxes and parameters M and P as the predictands. For a parameter X representing, M, P or the daytime surface fluxes, a second-order regression equation was determined for each case with the form

$$X = C_0 + C_1T_d + C_2T_d^2 + C_4T_n + C_5T_n^2, \quad (21)$$

where the coefficients C_0 to C_5 were calculated from the 16 sets of model results for the daytime and nighttime surface temperatures, T_d and T_n, respectively.

Our results indicate that M, P, and the fluxes varied monotonically and almost linearly with T_d and T_n over almost the entire range of values, the exceptions being at extreme values of M of P. The multiple correlation coefficient for these regression equa-

[6] Tests with the model indicate that the initial temperature profile within the ground is unimportant, within reasonable limits, in predicting afternoon or the following night temperatures. Over deep water, the model is inappropriate however, because of the essentially infinite heat storage capacity of the substrates. However, the values for the surface heat flux and for M appear to be reasonable over water.

tions was always close to 1.0. In instances of bivalued solutions, there was very little variation of X with temperature. Thus, except for isolated occasions with extreme values of M of P, the solutions were single valued.

Accordingly, the last step in the analysis procedure, as illustrated by the flow chart in Fig. 3, was to transform the rectified temperature images contained in the subset grid to maps of M, P, H_0 and E_0 (G_0 is henceforth not discussed). The transformation was done by substituting the measured temperatures into the regression equations for all grid points in the topo array. Because the day and night orbits were not exactly coincident, the topo subset area common to both working areas was necessarily smaller than either 130 × 130 working area, as illustrated in Fig. 4.

In initializing the model, the choice of surface parameters, other than M and P, and of the meteorological data was not critically important in determining T_0, although reasonable values of the wind speed, surface roughness, surface albedo, temperature, etc., were chosen to assure that the inferred values of M and P lay within reasonable limits for the observed ranges of daytime and nighttime temperatures.[7]

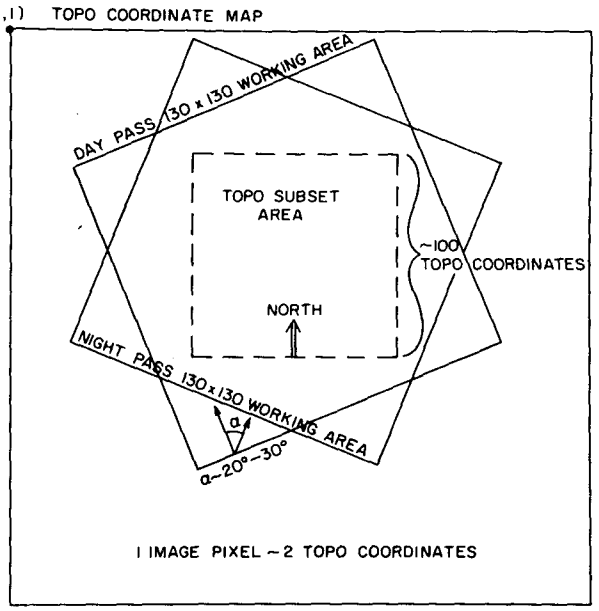

FIG. 4. Schematic representation of subset area.

5. Case studies

Satellite measurements for the two cases presented in this paper were obtained from two night/day pairs, 36 h apart over Los Angeles (30–31 May 1978) and St. Louis (9–10 June 1978). Nighttime orbits were made at about 0230 LST on the first day and daytime orbits at about 1330 LST on the following afternoon. Since the daytime temperature wave produces an effect on the nighttime temperature, simulations were always initiated at about 0600 LST model time. However, in order to minimize computer time, and because it is unrealistic to expect a one-dimensional model to give satisfactory results for periods much in excess of one day, we made the assumption that the surface temperature wave was stationary over a period of 36 h. We assumed stationarity in the temperature response between 30 and 31 May as a basis for reversing the ordering of day/night sequence in the model and for assuming a 12 h interval between orbits. In the Los Angeles case, the model was initialized at dawn on the 30th and allowed to proceed until nearly dawn on the 31st. However, the satellite passes were made at approximately 0230 LST 30 May and 1330 LST 31 May. In the St. Louis case the model was run for 36 h starting at dawn on 9 June, with daytime output during the afternoon of the 10th. The satellite passes were made at approximately 0230 LST 9 June and 1330 LST 10 June.

Justification for the artificial arrangement of orbits is based not simply on necessity but on the grounds that surface temperature under uniform weather conditions responds most sensitively to the nature of the terrain. Meteorological conditions were typical in both cases of a dry, mild, fair weather pattern with clear skies and weak advection; no rain had occurred for several days prior to the period. In looking at a number of other urban cases at different times of the year, we are struck by the overall similarity in surface-temperature patterns that characterize a particular urban area. The recurrence of these patterns suggests that surface effects more than the large-scale weather conditions govern the small-scale patterns of temperature under normal circumstances. Thus, we conclude that no serious complications arose from the reverse ordering of orbits.

a. Los Angeles 30 and 31 May 1978

The daytime (1330 LST 31 May) surface temperature map in Fig. 5 displays a large area centered on the cities of Maywood and Commerce where the ground temperatures were in excess of 32°C, warmer than at any other location within the Los Angeles Basin. Highest values, in excess of

[7] The value of the surface roughness z_0 used in these urban cases was 30 cm. Jason Ching of the Environmental Protection Agency has calculated from tower wind data from St. Louis a roughness length of between 60 and 120 cm. Our choice of 30 cm is likely to be close to an area average and well within an order of magnitude of the extreme values for the St. Louis area. We also chose a surface albedo of 18% which, according to our visible radiance measurements from the satellite, was within ±5% of the extreme values over most of the region.

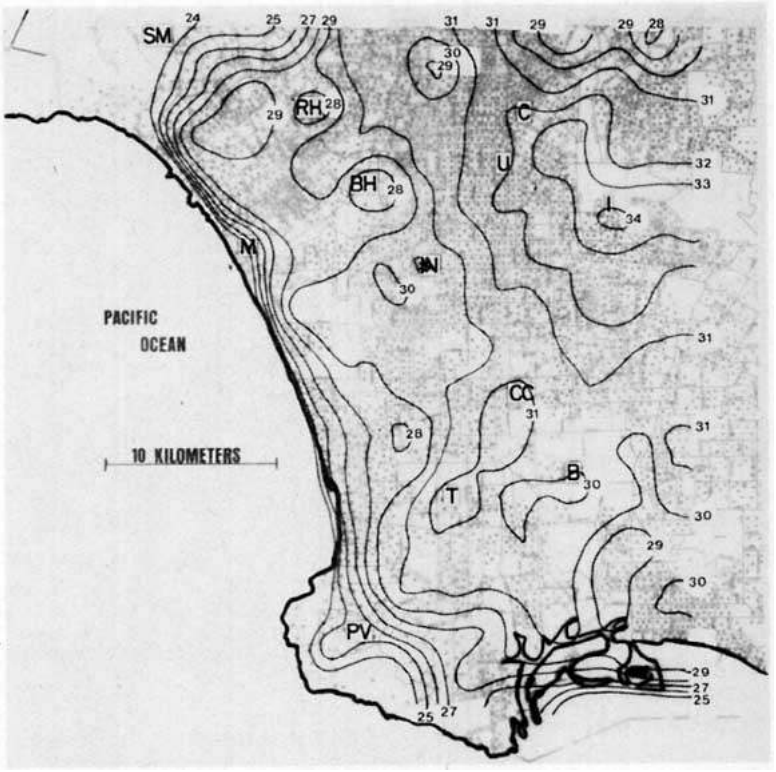

FIG. 5. Los Angeles, 31 May 1978 daytime (~1330 LST) surface temperature analysis. (Density of background shading represents population density.) This and subsequent temperature analyses have been determined from data measured aboard the NASA Heat Capacity Monitoring Mission (HCMM) Satellite. Units in °C.

34°C, are found over the Maywood industrial site (I) where commercial centers, railroads and heavy industry conglomerate to form a sizeable region in which there is almost no vegetation. The 32°C isotherm extends to the northwest of the industrial area to include the business district of downtown Los Angeles (C), an area 5–10 km on a side composed of high-rise office buildings, parking lots, and a dense intersecting network of streets. Other local temperature maxima are all related to business or industrial centers such as Compton (CC), the oil refinery sites near Torrance (T), and the commercial district in Bellflower (B).

The most obvious minimum appears just east of the strong gradient along the coast where the relatively cool ocean (15°C) bounds the beaches and coastal areas. Other prominent minima can be seen over the Santa Monica Mountains (SM), which border the Basin to the northwest, the hills immediately north of downtown, and the Palos Verdes Peninsula (PV). The notably lower temperatures (<22°C), evident at SM and PV, likely were due to the higher elevation as well as to the higher evaporation potential of these vegetated regions. On the urban plain itself, the only other apparent minima are found over large grassy areas which include Rancho-Hillcrest Park, Inglewood Country Club and the Baldwin Hills (RH, IN, BH). The temperature range over the lower density suburban residential areas, which comprise a majority of the Los Angeles Basin, was small.

The nighttime (0230 LST 30 May) pattern (Fig. 6) certainly is less well-defined than the daytime pattern with the range of temperatures between 10 and 13°C over the Basin. In general, temperatures 10–15 km inland were warmer than those near the coast, but this was more likely a direct reflection of an urban rather than a marine influence since the wind at night was a weak easterly drainage flow from land to sea.[8] The highest temperatures exceeded 13°C and were centered on a high population density business and residential area near the University of Southern California (USC) campus (U). Generally, regions which exhibited a warm daytime anomaly

[8] The lack of gradient near the coast is due to the fact that the ocean and land temperatures were very similar. There does seem to have been some gradient between the shallow coastal waters and the deeper ocean to the west.

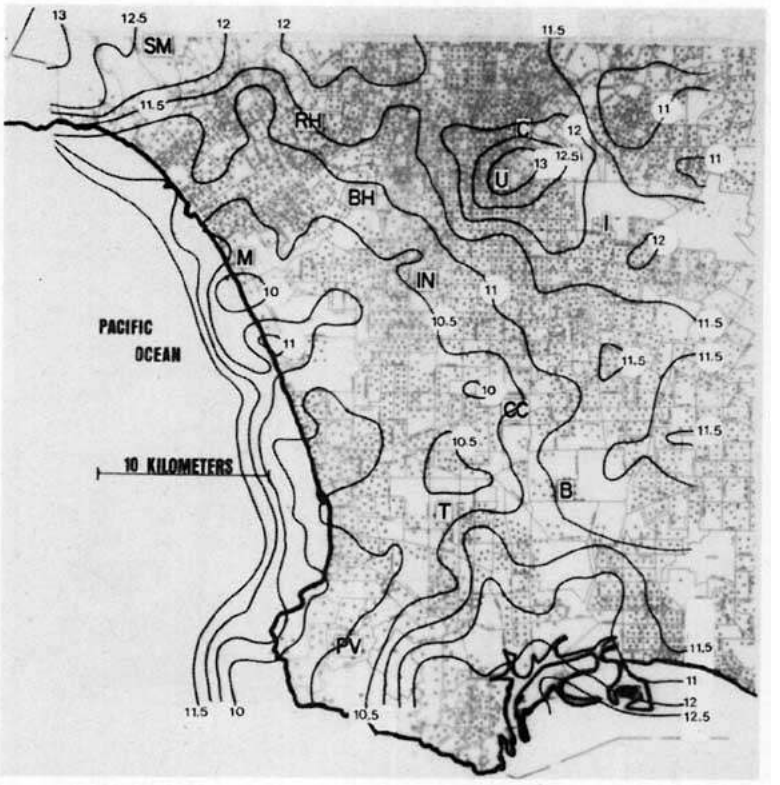

FIG. 6. Los Angeles, 30 May 1978 nighttime (~0230 LST) surface temperature analysis. Units in °C.

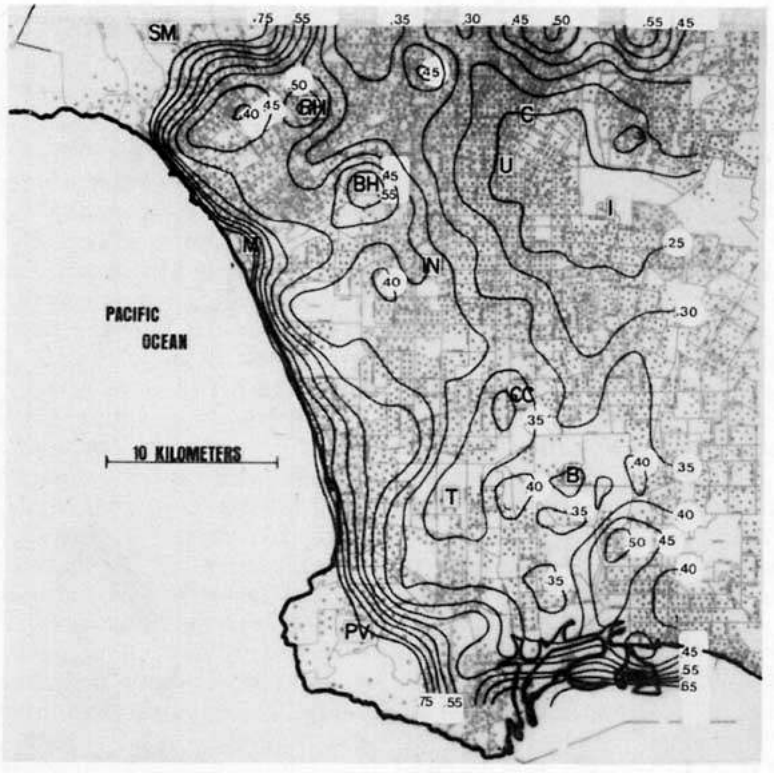

FIG. 7. Los Angeles moisture availability analysis for 30–31 May 1978.

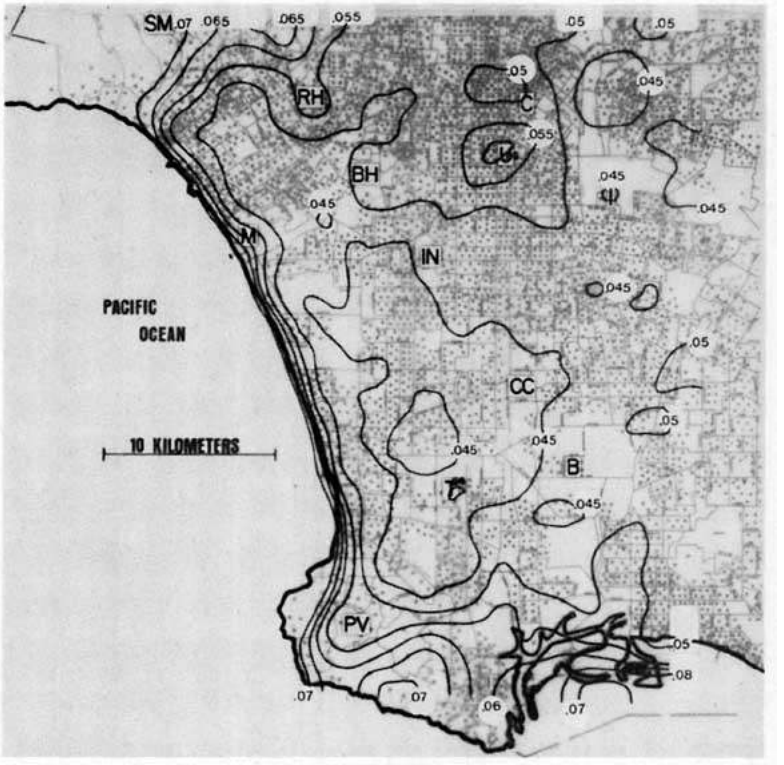

FIG. 8. Los Angeles thermal inertia analysis for 30–31 May 1978 (units in cal cm^{-2} K^{-1} $s^{-1/2}$).

tended to be warmer at night (areas I, C, and U), although this correspondence is weak.

The pattern of moisture availability M (Fig. 7) reveals a striking similarity to the daytime temperature map, M being inversely correlated with temperature. This inverse relationship is to be expected since a large evaporation potential results in a relatively small portion of the net radiation partitioned as sensible heat flux, a situation which translates into low surface temperatures. Conversely, lack of moisture for evaporation from dry ground allows greater surface heating. Values of M show a wide range across the domain, from 0.25 to 0.75. A large area below 0.25 is found over the Maywood industrial site (I), extending westward and northward to include most of the downtown business district (C). The surface fabric within this region is a heterogeneous mix of urban materials with vegetation or open fields larger than 1 acre almost nonexistent. Other local minima with M below 0.35 surround the Compton business district (CC), extending southwest to include the oil refineries near Torrance and Wilmington (T).

Local maxima of M are found over sparsely populated hilly areas of large parks scattered over the Los Angeles environs. The most prominent maxima include Rancho-Hillcrest Park (RH), the Baldwin Hills (BH), and the area of low population density centered on Signal Hill (south of B) near Long Beach. The Santa Monica Mountains (SM) and Palos Verdes Peninsula (PV) are large areas where the moisture availability was >0.5. The tendency for M to be higher in these areas is reasonable in view of the fact that both sites have small population densities and abundant vegetation. Since elevation effects are not included in the model some error is to be expected in these regions. However, an accurate representation of the spatial variations of heating is fundamentally more important in determining the atmospheric forcing than the exact values of the parameters at any point. As in the daytime temperature pattern (Fig. 5), the coastline again corresponds to a strong gradient in M although smoothing the data tends to weaken the strong gradient which otherwise would be discontinuous along the coast. In general, M values of ~0.7 for completely vegetated areas, 0.4 for suburban sites, and 0.3 or less for the industrial and commercial districts appear to be representative for the Los Angeles area in this case.

The map of thermal inertia (Fig. 8) appears to lack detail. This quantity was thought to vary significantly across an urban domain and has been presumed to be largely responsible for determining the nighttime urban temperature pattern. The values shown, however, reflect a rather small variability,

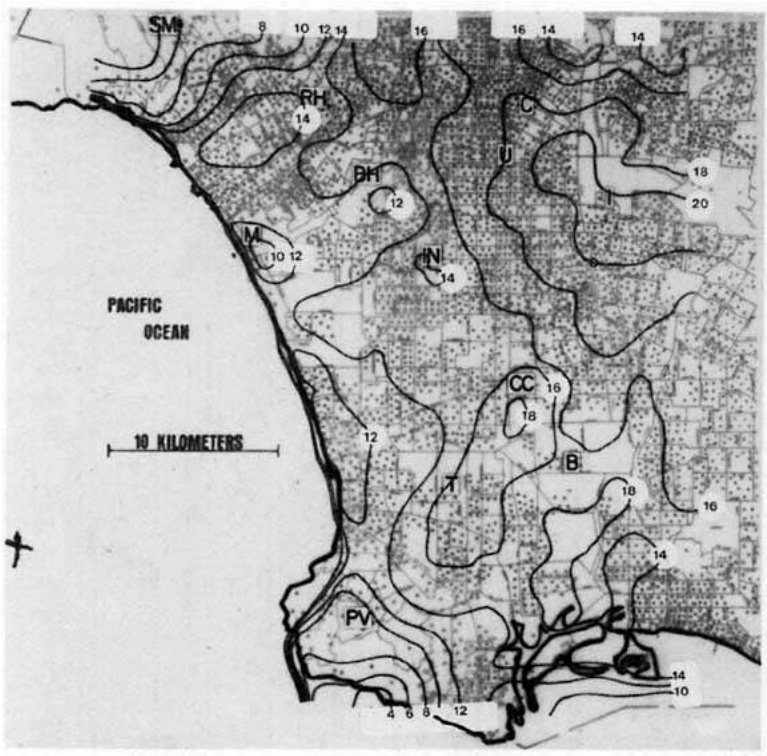

FIG. 9. Los Angeles surface sensible heat flux (W m^{-2} × 0.1) at approximately 1330 LST 31 May 1978 ($R_n \approx 630$ W m^{-2}).

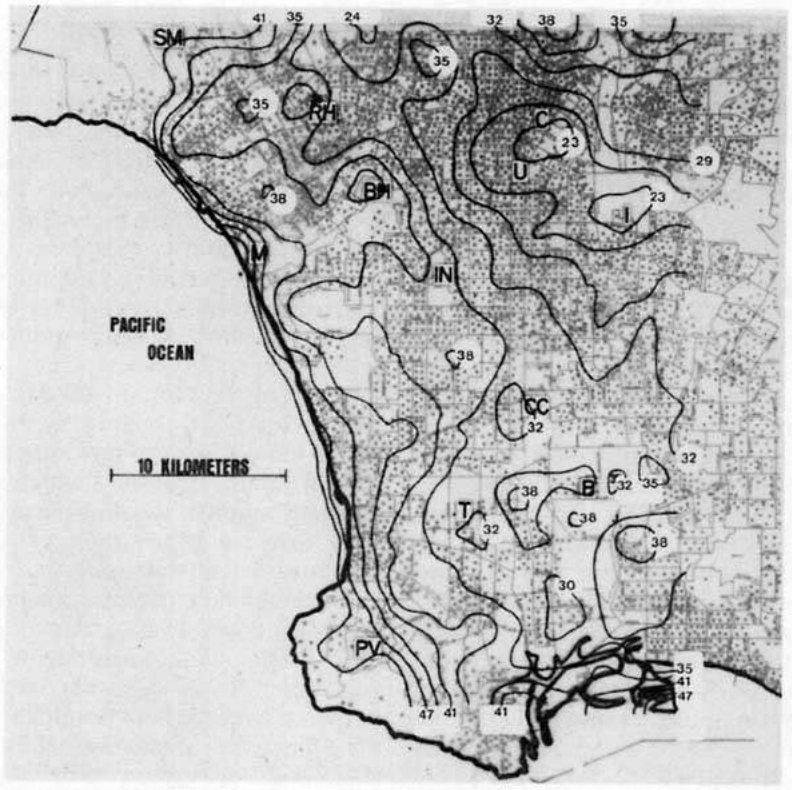

FIG. 10. Los Angeles surface moisture flux (W m^{-2} × 0.1) at approximately 1330 LST 30–31 May 1978 ($R_n \approx 630$ W m^{-2}).

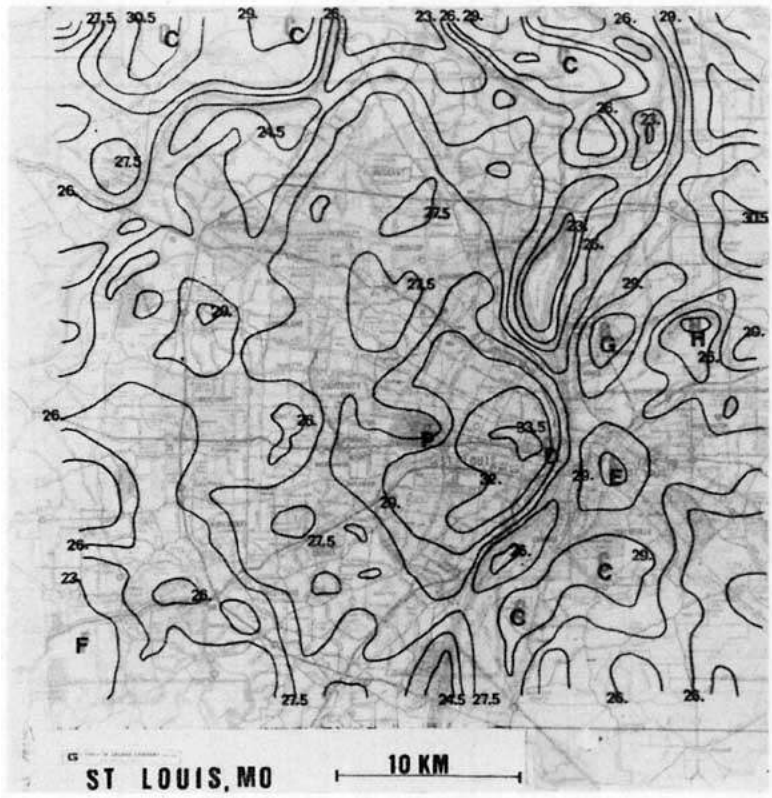

FIG. 11. St. Louis, 10 June 1978 daytime (~1330 LST) surface temperature analysis. Units in °C.

with P generally restricted between 0.04 and 0.05. The one obvious exception is a maximum centered near the USC campus (U) where $P > 0.06$. This is the same location that exhibited the maximum nighttime temperature anomaly and is quite close to the Los Angeles Civic Center (C). The pattern of P over the Santa Monica Mountains (SM) and Palos Verdes (PV) again appears to be somewhat distorted due to the elevation. However, a strong gradient coincides with the coastline, although smoothing of the data undoubtedly broadens the gradient near the coast.

Perhaps the most interesting analysis to be discussed is that of the surface heat flux, which is displayed in Fig. 9. This figure, showing the inferred surface heat flux at 1330 LST, offers a unique picture of the variation of H_0 across a heterogeneous urban domain. As anticipated, the maximum values appear centered in the same area where the largest daytime temperature anomaly is found, the 200 W m^{-2} contour enclosing almost exactly the same region as the 33°C contour in Fig. 5. A prominent maximum was located at the Compton commercial district (CC) extending southwest to the oil refinery site near Torrance (T).

Regions of relative minima, where the heat flux was approximately half that in the downtown area, are centered over the Baldwin Hills (BH) and at Marina Del Ray (M), the latter being a man-made marina which extends some distance inland. As with the daytime temperatures, the coastline again corresponds to a sharp gradient in the pattern.

The most general feature is the increase in flux between the coastline and interior, reflecting the land use pattern in which suburban tracts congregate near the coast while heavy industry and commercial centers are located inland. Thus, a striking relationship between urbanization and large sensible heat flux is quite apparent in this figure.

The map of surface moisture flux E_0 presented in Fig. 10 exhibits a pattern which is closely related to the distribution of the sensible heat flux over the Los Angeles Basin. In general, areas which are minima of H_0 appear as maxima of E_0 and vice versa. E_0 has a marked minimum over the commercial-industrial districts near downtown Los Angeles (U, I) with the lowest valued isopleths surrounding two areas where E_0 was below 230 W m^{-2}. The largest moisture fluxes occurred over the high terrain (SM and PV) and over the grassy open areas where the moisture availability (Fig. 7) also was found to be large. It is evident that the evaporation over less densely vegetated regions

FIG. 12. St. Louis, 9 June 1978 nighttime (~0230 CST) surface temperature analysis. Units in °C.

was relatively small, yet E_0 still exhibits values there which are as large as H_0 in regions where the latter is a maximum.

b. St. Louis, 9 and 10 June 1978

The map of daytime temperature (Fig. 11) displays a wide variation, with values ranging from 23°C to above 32°C. The three urban sites which show the highest temperatures include downtown St. Louis (D), East St. Louis across the river (E), and the industrial center of Granite City (G). Over these areas the ground temperatures varied from 30 to 34°C. Maximum temperatures were located near the City Hall and Memorial Plaza district where high-rise office buildings, parking lots, and a dense network of roads and highways comprise an urban ground fabric with little vegetation. Both East St. Louis and Granite City are also completely developed, with significant areas of heavy industry. Several other non-urban sites (identified by the letter C) exhibit daytime temperatures approaching or exceeding 30°C. All of these sites are separated from the urban centers by several kilometers and are located to the northwest, northeast and southeast of the city. Examination of U.S. Geological Survey land-use maps indicates that these areas consist of cropland (probably in an early stage of maturity) and pasture characterized by extensive areas of open field and low vegetation.

The water bodies [e.g., Horseshoe Lake (H)] are well defined by isopleths of lower temperature with the lowest isotherm being 23°C. Although actual river and lake temperatures varied from 15 to 19°C in the raw measurements, the smoothing of the data combined with the elimination of isotherms below a certain value tended to remove detail from the analysis around bodies of water such as the Mississippi River. The most evident ground temperature minima were centered in the southwest corner of the map (F) where a large expanse of deciduous trees remains despite the proximity of urbanization.

The nighttime range of temperature (3.5–6.5°C) presented in Fig. 12 indicates much smaller urban-versus-rural differences that those observed during the day. The St. Louis urban center possessed the highest temperatures. Values were above 6°C over the downtown area near the river, while in a significant region surrounding this area they exceeded 5.5°C. In comparison, typical rural temperatures varied from 4 to 5°C. The urban sites of East St. Louis (E) and Granite City (G), which correspond to

FIG. 13. St. Louis moisture availability analysis for 9–10 June 1978.

daytime maxima, do not display significant nighttime anomalies. Also, the cropland and pasture sites (C) which corresponded to daytime maxima were relatively cool at night, especially the areas to the southwest and southeast of the city where temperatures were below 4°C. The rivers and Horseshoe Lake (H) appear in the isotherm pattern as distinct temperature maxima in excess of 8°C.

The moisture availability (Fig. 13) reflects the remarkable variability in M across the working area, with values ranging from <0.2 over the downtown area to >0.9 over the forested region southwest of the city. The most obvious feature in this figure is certainly the marked reduction in the evaporation over the city, where a large area centered on the downtown district is enclosed by the 0.2 contour and is almost coincident with the same region defined by the 32°C contour on the daytime temperature map. East St. Louis (E) and Granite City (G) also appear as M minima. Other sites which correspond to M values below 0.3 are the pasture-cropland (C) areas where the vegetation was sparse and short, allowing for strong heating of the surface during the day.

The only pronounced maximum of M (apart from the rivers and lakes) coincided with the forested region (F) in the far southwestern corner of the map where the moisture availability locally exceeded 0.9. Thus M has a wide variability across the domain and is inextricably related to land use and particularly to vegetation type. The average range of M was generally between 0.3 and 0.6.

As with Los Angeles, the spatial distribution of thermal inertia (Fig. 14) was unexpectedly indistinct. The rivers and Horseshoe Lake are delineated by large values of P. Across most of the map, the variation of P is minimal, with values mostly between 0.025 and 0.035. The only discernible pattern appears at the cropland-pasture sites (C) where three minima of P below 0.025 are identifiable. Although the surfaces of these areas were quite hot during the day, their relative inability to conduct heat downward and store it during the day and conduct it to the surface at night is typical of a surface fabric with low thermal inertia.

Fig. 15 presents a representation of the spatial variation of H_0 at the time of the afternoon orbit. The St. Louis downtown area is enclosed by the 250 W m^{-2} contour which closely coincides with the location of the 32°C daytime isotherm. A large area where the flux is found to exceed 230 W m^{-2} surrounding this region includes the commercial and industrial districts near the city center. The other urban sites of east St. Louis (E) and Granite City (G) also reflect the significant alteration that urban

FIG. 14. St. Louis thermal inertia analysis for 9–10 June 1978 (units in cal cm^{-2} K^{-1} $s^{-1/2}$).

substrates impose on the energy balance compared with suburban or densely vegetated areas. The other maxima appear at the cropland sites (C) that surround the suburbs of the city. The magnitude of H_0 appears as large at these locations as in the most built-up areas, where values also exceeded 250 W m^{-2}. For most of the area outside the heavily urbanized areas H_0, varied from 150 to 200 W m^{-2}, with the smallest heat flux located over vegetated areas such as the forested region (F) southwest of the city.

The map of surface moisture flux E_0 (Fig. 16) displays a distribution that closely corresponds to the fields of moisture availability and sensible heat flux shown in Figs. 13 and 15. The downtown area (D) exhibits a strong minimum where an isopleth encloses a region over which E_0 is <260 W m^{-2}. This is the same area where M was smallest and H_0 largest. The two other large urban sites (E, G) and the cropland-pasture areas (C) also appear as relative minima of E_0, reflecting the strong influence which vegetation exercises on the surface energy balance. The moisture flux was largest over vegetation such as the forested area southwest of the city where E_0 exceeded 500 W m^{-2}. Interestingly, as was the case with Los Angeles, the smallest values of E_0 were larger than the maximum sensible heat flux, suggesting that the vegetation cover over urban areas is still sufficient to provide ample moisture flux.

6. Discussion

The maps of temperature, moisture availability, thermal inertia, and daytime heat and moisture flux across the areas centered on the cities of Los Angeles and St. Louis should aid in understanding the mechanisms responsible for the creation and maintenance of the urban heat island. The daytime spatial variation of temperature is especially impressive with the city centers as much as 10°C warmer than nearby rural areas. Both St. Louis and Los Angeles exhibit well-defined maxima centered on the commercial and industrial districts near the downtown areas, a pattern which reflects the strong influence that land use plays in influencing the surface response to the solar forcing. Temperature minima consistently appear in locations with significant vegetation. Various grasscovered hilly areas scattered across the Los Angeles Basin and the forested region southwest of St. Louis all appear as sites where the surface temperature was distinctly lower than over urban areas just a few kilometers away.

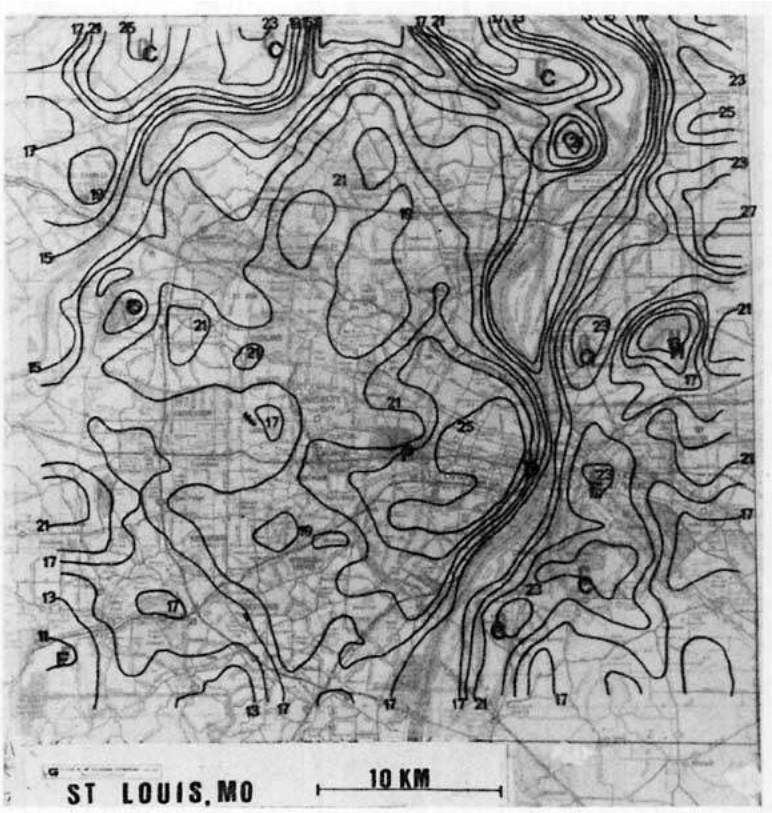

FIG. 15. St. Louis surface sensible heat flux (W $m^{-2} \times 0.1$) at approximately 1330 CST 10 June 1978 ($R_n \approx 640$ W m^{-2}).

The patterns of moisture availability also show similarly clear relation to terrain, specifically a reduction of M over urban and sparsely vegetated areas. Over both St. Louis and Los Angeles, minima of M center directly on the downtown commercial sites where the urban fabric is a heterogeneous mixture of asphalt and concrete with few freely transpiring surfaces. The moisture budget over cities thus reflects an artificial alteration of the substrate. Suburban regions consistently exhibit values of moisture availability between 0.3 and 0.5, values which seem to be typical for the overall region. The largest evaporation potential is found over grassy park areas in Los Angeles and the forested region southwest of St. Louis, which had a moisture availability above 0.8, a value that seems reasonable over a completely vegetated site. The wide range of M values again reflects the profound effect that land cover variations have in influencing urban microclimates.

The patterns of thermal inertia were more difficult to interpret. It was expected that P would show a wide variation across the working area, with distinct maxima near the city centers reflecting the enhanced ability of urban substrate materials to store and conduct heat. Both Los Angeles and St. Louis, however, failed to show any significant elevation of thermal inertia in the downtown districts. The only strong exception is a site west of Los Angeles where a local maximum of P is found. Some one- to four-story structures dominate this area, but the land use would not seem to be significantly different from that in other high population density districts nearby. Therefore, it is not immediately apparent why the thermal inertia should be higher at this particular location. The only readily understandable feature in the pattern of P appears on the St. Louis map over the pasture-cropland sites surrounding the perimeter of the city. Here there is a clear pattern of lower values of thermal inertia. It seems reasonable that open areas of short vegetation or bare soil should store less heat than fully vegetated or urbanized surface, although such small variations as shown in the figures for Los Angeles and St. Louis may be due to variations in the other terrain parameters that are presumed constant in the model.

Maps of the surface heat and moisture flux were the most interesting since these figures represent H_0 and E_0 very near the time of maximum flux. As expected, the urban centers correspond to H_0 maxima where the heat flux was two to three times greater than over more vegetated areas nearby. Both downtown St. Louis and Los Angeles exhibit local values

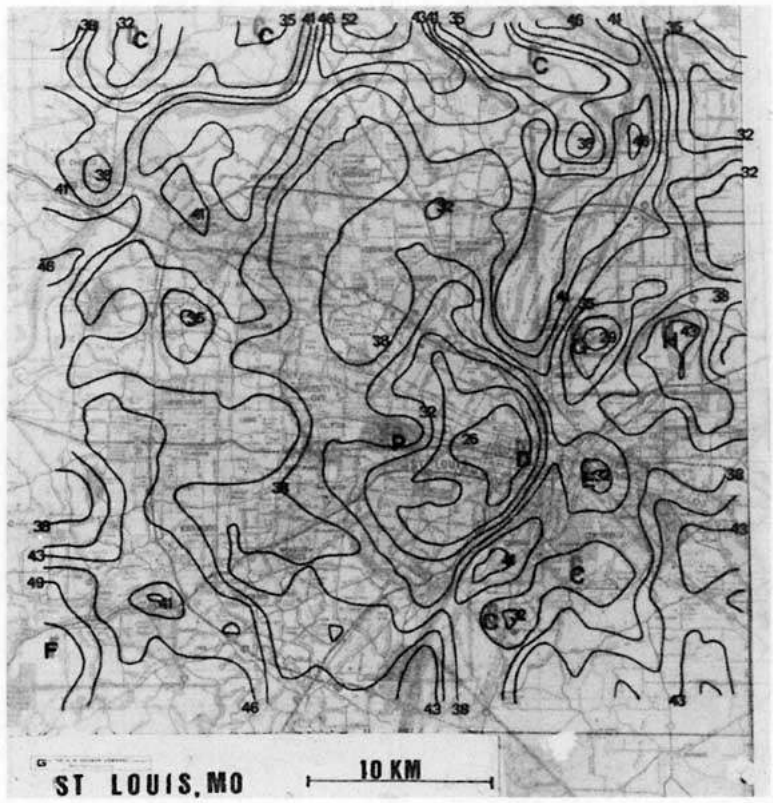

FIG. 16. St. Louis surface moisture flux (W m^{-2} × 0.1) at approximately 1330 CST 10 June 1978 ($R_n \approx 640$ W m^{-2}).

of H_0 in excess of 250 W m^{-2} and Bowen ratios of about 1.0, while over densely vegetated areas H_0 was below 100 W m^{-2} and the Bowen ratio ~ 0.2. The complexity of the heat flux pattern is evident in the unsmoothed enlargement of the St. Louis downtown district (Fig. 17) where Forest Park (FP) is seen to have a heat flux roughly half that of the city center just a few kilometers away.

Over St. Louis, analyses show that the largest daytime heat flux values occurred over a corridor lying between the southern business district of St. Louis and Granite City to the northeast, the same area where METROMEX investigators found the strongest boundary-layer convergence (Kropfli and Kohn, 1978; Wong and Dirks, 1978) and the location of the earliest radar echoes and most disturbed convective situations during conditions of air mass thunderstorms (Braham and Dungey, 1978, Braham and Wilson, 1978). Thus, seems quite likely that urban precipitation anomalies are closely linked to the pattern of surface heating.

7. Conclusions

A procedure has been developed which uses satellite-derived surface temperature fields in combination with output from a numerical model of the boundary layer to infer the spatial distribution of the effective surface parameters, M (moisture availability) and P (thermal inertia), and the sensible and evaporative heat fluxes at the surface. The approach is general and may be applied to any surface for which ground temperature data is available and over which horizontal homogeneity of large-scale meteorological features may be assumed. Maps of M, P, and the sensible and latent heat fluxes at the surface are presented for two urban cases, Los Angeles and St. Louis.

P and M have been proposed as the two parameters that are most responsible for the temperature variations over a rural-urban complex (Carlson and Boland, 1978). The present research suggests that M is the governing parameter during the day, when urban centers coincide with distinct minima and suburban and rural areas possess values in excess of 0.5. The areas of daytime temperature maxima all correspond quite closely to minima in moisture availability. However, thermal inertia patterns were surprisingly ill-defined. We had anticipated that both Los Angeles and St. Louis would exhibit maxima in P, reflecting the enhanced ability of the urban substrate to store and conduct heat. Although both cities were relatively warm at night, P did not exhibit significant elevations in either location. Thus, the ele-

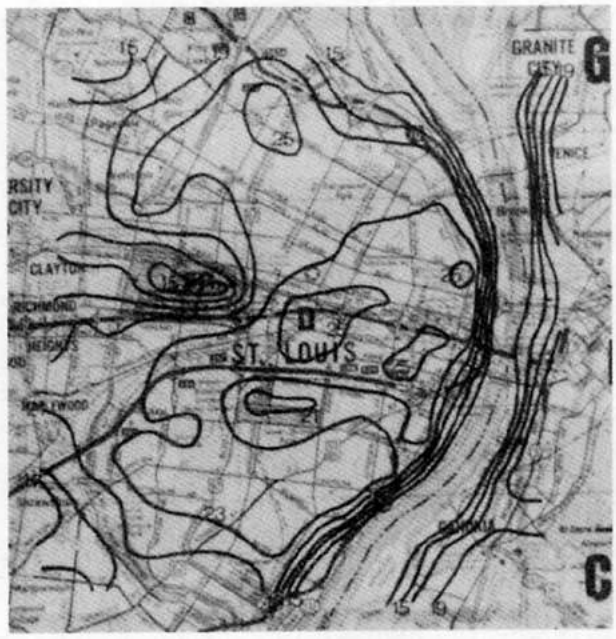

FIG. 17. Enlargement of unsmoothed surface heat flux (W m^{-2} × 0.1) over downtown St. Louis at approximately 1330 LST 10 June 1978.

vated nighttime temperatures over both St. Louis and Los Angeles are explainable not by elevated surface conductivity but by greater daytime heat storage due to lower values of M. This conclusion is intriguing and differs from previous suppositions concerning the distribution of P over the urban-rural complex.

The mapping of the sensible and evaporative heat fluxes at the surface have visibly demonstrated the alteration of the surface energy balance by cities. Both urban centers appear as distinct maxima of H_0 and minima of E_0, and these regions correspond very closely with the sites of highest daytime temperature. In METROMEX, the region around St. Louis that experienced the strongest surface warming and low-level convergence lay within a corridor between the city center and Granite City and East St. Louis across the river. In this study (and in other cases not presented), this region proved also to possess the largest values of surface heat flux. We conclude that enhanced warming of the urban boundary layer results in differential heating patterns that drive the small-scale circulations. If so, the summertime urban heat island must then be directly attributable to the presence of surfaces that do not retain moisture; therefore, human alteration of the surface, and especially the lack of a vegetation cover, constitute a root cause of this urban weather anomaly.

The combination of modeling and remote sensing techniques described in this paper holds promise for a variety of practical applications. The spatial variation of E_0, H_0, M or P could constitute an important input to mesoscale models for investigating the dynamic response of the atmosphere to urban modifications. Presently, the terrain parameters such as M and P are crudely estimated or entirely neglected in boundary-layer components of large-scale models. In particular, the derivation of heat flux over inhomogeneous terrain may be especially useful in modeling the boundary-layer height and the turbulent fluctuations within the mixed layer. Evaporation and moisture availability maps may also provide information for use in agriculture and hydrology.

Acknowledgments. We are indebted to Dr. Alfred K. Blackadar for allowing us to use portions of his slab model. The authors also wish to thank the Environmental Protection Agency (EPA) and the National Aeronautics and Space Administration (NASA) for sponsoring this research, respectively, under Grants R-805640020 and NAS-5-24264.

REFERENCES

Blackadar, A. K., 1979: High resolution models of the planetary boundary layer. *Advances in Environmental Science and Engineering*, Vol. I, *Fundamentals*, J. R. Pfafflin and E. N. Ziegler, Eds., Gordon and Breach, 276 pp.

Braham, R. R., and D. Wilson, 1978: Effects of St. Louis on convective cloud heights. *J. Appl. Meteor.*, **17**, 587–599.

——, and M. J. Dungey, 1978: A study of urban effects on radar first echoes. *J. Appl. Meteor.*, **17**, 644–654.

Carlson, T. N., and F. E. Boland, 1978: Analysis of urban-rural canopy using a surface heat flux/temperature model. *J. Appl. Meteor.*, **17**, 998–1013.

——, J. A. Augustine and F. E. Boland, 1977: Potential application of satellite temperature measurements in the analyses of land use over urban areas. *Bull. Amer. Meteor. Soc.*, **96**, 91–114.

Chandler, T. J., 1976: Urban climatology and its relevance to urban design. WMO Tech. Note, No. 438, No. 149, 61 pp.

Changnon, S. A., 1969: Recent studies of urban effects on precipitation in the United States. *Bull. Amer. Meteor. Soc.*, **50**, 411.

——, 1978: Urban effects on severe local storms at St. Louis. *J. Appl. Meteor.*, **17**, 578–586.

Chen, E., L. H. Allen, Jr., J. F. Bartholic, R. G. Bill, Jr. and R. A. Sutherland, 1979: Satellite-sensed winter nocturnal temperature patterns of the Everglades agricultural area. *J. Appl. Meteor.*, **18**, 992–1002.

Cogan, J. L. and J. H. Willand, 1976: Measurement of sea surface temperature by the NOAA-2 satellite. *J. Appl. Meteor.*, **15**, 173–180.

Dabberdt, W. F. and P. A. Davis, 1978: Determination of energetic characteristics of urban rural surfaces in the greater St. Louis area. *Bound.-Layer Meteor.*, **14**, 105–121.

Deardorff, J. W., 1978: Efficient prediction of ground surface temperature and moisture with inclusion of a layer of vegetation. *J. Geophys. Res.*, **83**, 1889–1903.

Duckworth, F. S., and J. Sandberg, 1954: The effect of cities upon horizontal and vertical temperature gradients. *Bull. Amer. Meteor. Soc.*, **35**, 198–207.

Garratt, J. R., 1978: Transfer characteristics for a heterogeneous surface of large aerodynamic roughness. *Quart. J. Roy. Meteor. Soc.*, **104**, 491–502.

Huff, F. A. and J. L. Vogel, 1978: Urban, topographic and diurnal effects on rainfall in the St. Louis region. *J. Appl. Meteor.*, **17**, 565–577.

Kahle, A., 1977: A simple thermal model of the earth's surface

for geologic mapping by remote sensing. *J. Geophys. Res.*, **82,** 1673–1680.

Kropfli, R. A. and N. M. Kohn, 1978: Persistant horizontal rolls in the urban mixed layer as revealed by dual-Doppler radar. *J. Appl. Meteor.*, **17,** 669–676.

Landsberg, H. E., 1956: *The Climate of Towns in Man's Role in Changing the Face of the Earth.* The University of Chicago Press, 584–606.

Manual of Remote Sensing II, 1975: American Society of Photogrammetry, Falls Church, VA, 867 pp.

Matson, M., E. P. McClain, D. McGinnis, Jr., and J. Pritchard, 1978: Satellite detection of urban heat islands. *Mon. Wea. Rev.*, **106,** 1725–1734.

Mellor, G. L. and T. Yamada, 1974: A hierarchy of turbulence closure models for planetary boundary layers. *J. Atmos. Sci.*, **131,** 1791–1806.

Monteith, J. L., 1961: An empirical method for estimating long-wave radiation exchanges in the British Isles. *Quart. J. Roy. Meteor. Soc.*, **87,** 171–179.

Monteith, J. L., 1975: *Vegetation and the Atmosphere*, Vol. I, *Principles*. Academic Press, 278 pp.

Myrup, L. O., 1969: A numerical model of the urban heat island. *J. Appl. Meteor.*, **8,** 908–918.

Nappo, C. J., 1975: Parameterization of surface moisture and evaporation rate in a planetary boundary layer model. *J. Appl. Meteor.*, **14,** 289–296.

Oke, T. R., 1974: Review of urban climatology, 1968–1973. WMO Tech. Note, No. 134, 61 pp.

Outcalt, S. I., 1972: The development and application of a simple digital surface-climate simulator. *J. Appl. Meteor.*, **11,** 629–636.

Rao, P. K., 1972: Remote sensing of urban heat islands from an environmental satellite. *Bull. Amer. Meteor. Soc.*, **53,** 647–648.

Rosema, A., 1979: A mathematical model for simulation of the thermal behavior of bare soils, based on heat and moisture transfer. Netherlands Tech. Memo. Series, Publ. No. 11, Delft, The Netherlands.

Sellers, W. D., 1965: *Physical Climatology*. The University of Chicago Press, 272 pp.

Soer, G. J. R., 1977: The Tergra model, a mathematical model for the simulation of the daily behavior of crop surface temperature and actual evapotranspiration. Netherlands Tech. Memo. Series, Publ. No. 46, Delft, The Netherlands.

——, 1980: Estimation of regional evapotranspiration and soil moisture conditions using remotely sensed crop surface temperatures. *Remote Sensing Environ.*, **9,** 27–45.

Shreffler, J., 1979: Urban-rural differences in tower-measured winds, St. Louis. *J. Appl. Meteor.*, **18,** 829–835.

Tanner, C. B., and W. G. Pelton, 1960: Potential evapotranspiration estimates by the approximate energy balance method of Penman. *J. Geophys. Res.*, **65,** 3391–3412.

Tennekes, H., 1970: Free convection in the turbulent Ekman layer of the atmosphere. *J. Atmos. Sci.*, **27,** 1027–1034.

——, 1973: A model for the dynamics of the inversion above a convective boundary layer. *J. Atmos. Sci.*, **30,** 558–567.

Wong, K. K. and R. A. Dirks, 1978: Mesoscale perturbations on airflow in the urban mixing layer. *J. Appl. Meteor.*, **17,** 677–688.